

Research Paper

Analysis of Two Lengthwise Cracks in a Viscoelastic Inhomogeneous Beam Structure

Victor Iliev RIZOV

Department of Technical Mechanics
University of Architecture, Civil Engineering and Geodesy
1 Chr. Smirnensky Blvd., 1046 – Sofia, Bulgaria
e-mail: v_rizov_fhe@uacg.bg

The present paper considers the time-dependent fracture in a continuously inhomogeneous viscoelastic cantilever beam with two lengthwise cracks. Time-dependent analytical solutions to the strain energy release rate, which take into account the viscoelastic behaviour of the material, are derived. A rheological model with two springs and two dashpots is used for studying the viscoelastic behaviour of the beam. A stress-strain-time relationship is obtained for the case when the rheological model is loaded by stress that increases linearly with time up to a certain level and then it remains constant. The variation of the strain energy release rate with time is analysed.

Key words: inhomogeneous beam; viscoelastic behaviour; lengthwise crack.

1. INTRODUCTION

The development in various areas of up-to-date engineering necessitates the application of more efficient continuously inhomogeneous structural materials. This type of materials is characterised by the continuous variation of material properties along one or more spatial directions in the solid. In fact, the continuously inhomogeneous (functionally graded) materials are composites consisting of several constituent materials that are mixed continuously during the manufacturing process [1–6]. The continuously inhomogeneous materials show certain advantages over the homogeneous structural materials. For example, graded distribution of the properties of the continuously inhomogeneous materials can be formed technologically. In this way, requirements for different material properties in different parts of a structural member can be met. The attention that has been paid to the continuously inhomogeneous materials by the international academic community in the recent decades is due primarily to the vital role played

by the functionally graded materials in such important areas as aerospace, nuclear power plants, microelectronics and biomedicine.

The safety and reliability of continuously inhomogeneous structural members and components depend to a large degree on their fracture behaviour. Therefore, analyses of various crack problems in continuously inhomogeneous materials are of key importance for the design and application of these novel composite materials. Since continuously inhomogeneous (functionally graded) materials can be built-up layer by layer [7, 8], there is a high risk of appearance of the lengthwise crack between layers. This fact emphasizes the need for studying lengthwise fracture behaviour of continuously inhomogeneous structures. Therefore, the present paper deals with the analysis of the time-dependent strain energy release rate for two lengthwise cracks in a viscoelastic continuously inhomogeneous beam configuration loaded by bending moments that are functions of time. It should be mentioned that the previous papers are focused on the instantaneous lengthwise fracture of continuously inhomogeneous beams subjected to loading that does not change with time [9, 10]. In other words, the novelty of the present paper is in the fact that viscoelastic behaviour under loading which changes with time is considered when deriving the strain energy release rate.

2. VISCOELASTIC INHOMOGENEOUS BEAM WITH TWO LENGTHWISE CRACKS

A continuously inhomogeneous viscoelastic cantilever beam configuration is depicted in Fig. 1. The beam is clamped in section Q . The cross-section of

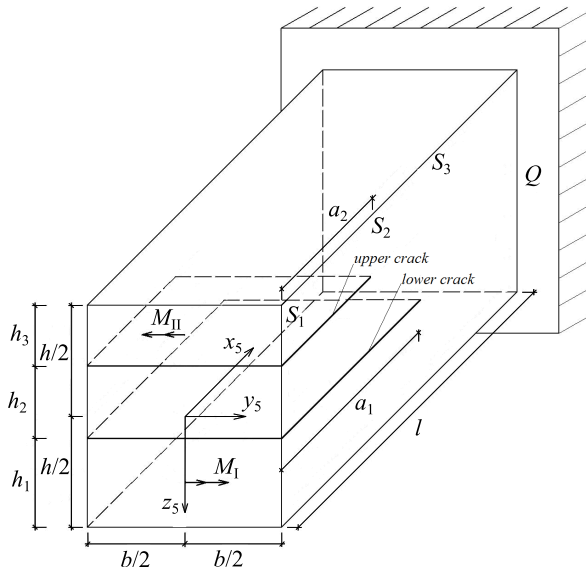


FIG. 1. Geometry and loading of a viscoelastic beam with two lengthwise cracks.

the beam is a rectangle of width b , and thickness h . The beam length is l . Two lengthwise cracks are located in the beam as shown in Fig. 1. The lengths of the lower and upper cracks are a_1 and a_2 , respectively, where $a_1 > a_2$. In the beam portion S_1S_2 , the cracks divide the beam into three crack arms. The thicknesses of the lower, middle and upper crack arms are denoted by h_1 , h_2 , and h_3 , respectively. In the beam portion S_2S_3 , the lower crack divides the beam into lower and upper crack arms with thicknesses, h_1 and h_4 , respectively, where $h_4 = h_2 + h_3$. The beam is loaded in bending by two moments M_I and M_{II} , applied at the free ends of the lower and upper crack arms, respectively. At $0 \leq t \leq t_1$, the two bending moments increase linearly with time

$$(2.1) \quad M_I = v_I t,$$

$$(2.2) \quad M_{II} = v_{II} t,$$

where t is time, v_I and v_{II} are the velocities of M_I and M_{II} , respectively. At $t \geq t_1$, the moments are constant

$$(2.3) \quad M_I = v_I t_1,$$

$$(2.4) \quad M_{II} = v_{II} t_1.$$

It is obvious that the middle crack arm is free of stresses (Fig. 1).

The viscoelastic behaviour of the beam is examined by using the rheological model shown schematically in Fig. 2. The model consists of a unit with one linear spring with the modulus of elasticity E_B , and two linear dashpots with coefficients of viscosity η_D and η_L . A second linear spring with the modulus of elasticity E_H is connected consecutively to the unit as shown in Fig. 2.

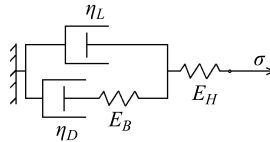


FIG. 2. Rheological model.

The stress-strain-time relationship for the rheological model in Fig. 2 is derived in the following manner. First, the equations for equilibrium are written as

$$(2.5) \quad \sigma_L + \sigma_B = \sigma,$$

$$(2.6) \quad \sigma_D + \sigma_L = \sigma,$$

where σ_B is the stress in the spring with the modulus of elasticity, E_B . The stresses in the dashpots with coefficients of viscosities η_D and η_L are denoted by σ_D and σ_L , respectively.

The dependence between strains is expressed as

$$(2.7) \quad \varepsilon_B + \varepsilon_D = \varepsilon_L,$$

where ε_B , ε_D and ε_L are the strains in the spring with the modulus of elasticity E_B , and in the dashpots with coefficients of viscosities η_D and η_L , respectively.

The stresses are expressed as functions of strains by Hooke's law

$$(2.8) \quad \sigma_B = E_B \varepsilon_B,$$

$$(2.9) \quad \sigma_D = \eta_D \dot{\varepsilon}_D,$$

$$(2.10) \quad \sigma_L = \eta_L \dot{\varepsilon}_L.$$

At $0 \leq t \leq t_1$, the stress σ increases with time at a constant velocity v , i.e.,

$$(2.11) \quad \sigma = vt.$$

By combining (2.5)–(2.11), one obtains

$$(2.12) \quad \eta_L \ddot{\varepsilon}_L + E_B \dot{\varepsilon}_L - \frac{E_B}{\eta_D} (vt - \eta_L \dot{\varepsilon}_L) = v.$$

The solution of (2.12) is derived as

$$(2.13) \quad \varepsilon_L = \frac{v}{\theta^2} \left(\frac{1}{\eta_L} - \frac{\beta}{\theta} \right) (e^{-\theta t} - 1) + \frac{\beta v}{2\theta} t^2 + \frac{v}{\theta} \left(\frac{1}{\eta_L} - \frac{\beta}{\theta} \right) t,$$

where

$$(2.14) \quad \theta = \frac{E_B}{\eta_L} \left(1 + \frac{\eta_L}{\eta_D} \right),$$

$$(2.15) \quad \beta = \frac{E_B}{\eta_D \eta_L}.$$

The strain in the spring with the modulus of elasticity E_H is written as

$$(2.16) \quad \varepsilon_H = \frac{vt}{E_H}.$$

By adding (2.16) to (2.13), one obtains

$$(2.17) \quad \varepsilon = \frac{v}{\theta^2} \left(\frac{1}{\eta_L} - \frac{\beta}{\theta} \right) (e^{-\theta t} - 1) + \frac{\beta v}{2\theta} t^2 + \frac{v}{\theta} \left(\frac{1}{\eta_L} - \frac{\beta}{\theta} \right) t + \frac{vt}{E_H}.$$

By combining (2.11) and (2.17), one derives

$$(2.18) \quad \sigma = \frac{\sigma}{\theta^2 t} \left(\frac{1}{\eta_L} - \frac{\beta}{\theta} \right) (e^{-\theta t} - 1) + \frac{\beta \sigma}{2\theta} t + \frac{\sigma}{\theta} \left(\frac{1}{\eta_L} - \frac{\beta}{\theta} \right) + \frac{\sigma}{E_H}.$$

Formula (2.18) represents the stress-strain-time relationship for the rheological model in Fig. 2 at $0 \leq t \leq t_1$.

The stress σ , does not change with time at $t \geq t_1$, i.e.

$$(2.19) \quad \sigma = vt_1.$$

Therefore, by considering the equilibrium of the components of the model in Fig. 2 one obtains

$$(2.20) \quad \eta_L \ddot{\varepsilon}_L + E_B \dot{\varepsilon}_L - \frac{E_B}{\eta_D} (\sigma - \eta_L \dot{\varepsilon}_L) = 0.$$

Equation (2.20) is solved as

$$(2.21) \quad \varepsilon_L = \sigma \xi - \frac{\delta \sigma - \theta \sigma \zeta}{\theta^2} - \frac{\delta \sigma}{\theta} t_1 + \frac{\delta \sigma - \theta \sigma \zeta}{\theta^2 e^{-\theta t_1}} e^{-\theta t} + \frac{\delta \sigma}{\theta} t,$$

where

$$(2.22) \quad \xi = \frac{1}{\theta^2 t_1} \left(\frac{1}{\eta_L} - \frac{\beta}{\theta} \right) (e^{-\theta t_1} - 1) + \frac{\beta}{2\theta} t_1 + \frac{1}{\theta} \left(\frac{1}{\eta_L} - \frac{\beta}{\theta} \right),$$

$$(2.23) \quad \zeta = -\frac{1}{\theta t_1} \left(\frac{1}{\eta_L} - \frac{\beta}{\theta} \right) e^{-\theta t_1} + \frac{\beta}{2\theta} + \frac{1}{\theta t_1} \left(\frac{1}{\eta_L} - \frac{\beta}{\theta} \right),$$

$$(2.24) \quad \delta = \frac{E_B}{\eta_L \eta_D}.$$

The strain in the spring with the modulus of elasticity E_H is found as

$$(2.25) \quad \varepsilon_H = \frac{\sigma}{E_H}.$$

The stress-strain-time relationship at $t \geq t_1$ is obtained by adding (2.25) to (2.21)

$$(2.26) \quad \varepsilon = \sigma \xi - \frac{\delta \sigma - \theta \sigma \zeta}{\theta^2} - \frac{\delta \sigma}{\theta} t_1 + \frac{\delta \sigma - \theta \sigma \zeta}{\theta^2 e^{-\theta t_1}} e^{-\theta t} + \frac{\delta \sigma}{\theta} t + \frac{\sigma}{E_H}.$$

Since the beam exhibits continuous material inhomogeneity in width, thickness and length directions, the material properties involved in the rheological model in Fig. 2 vary continuously in the volume of the beam. The continuous variations of E_B , η_D , η_L , and E_H in the beam cross-section are written as

$$(2.27) \quad E_B = E_{B0} + \frac{E_{B1} - E_{B0}}{b^{m_1}} \left(\frac{b}{2} + y_5 \right)^{m_1} + \frac{E_{B2} - E_{B0}}{h^{m_2}} \left(\frac{h}{2} + z_5 \right)^{m_2},$$

$$(2.28) \quad \eta_D = \eta_{D0} + \frac{\eta_{D1} - \eta_{D0}}{b^{n_1}} \left(\frac{b}{2} + y_5 \right)^{n_1} + \frac{\eta_{D2} - \eta_{D0}}{h^{n_2}} \left(\frac{h}{2} + z_5 \right)^{n_2},$$

$$(2.29) \quad \eta_L = \eta_{L0} + \frac{\eta_{L1} - \eta_{L0}}{b^{p_1}} \left(\frac{b}{2} + y_5 \right)^{p_1} + \frac{\eta_{L2} - \eta_{L0}}{h^{p_2}} \left(\frac{h}{2} + z_5 \right)^{p_2},$$

$$(2.30) \quad E_H = E_{H0} + \frac{E_{H1} - E_{H0}}{b^{q_1}} \left(\frac{b}{2} + y_5 \right)^{q_1} + \frac{E_{H2} - E_{H0}}{h^{q_2}} \left(\frac{h}{2} + z_5 \right)^{q_2},$$

where

$$(2.31) \quad -\frac{b}{2} \leq y_5 \leq \frac{b}{2},$$

$$(2.32) \quad -\frac{h}{2} \leq z_5 \leq \frac{h}{2}.$$

In formulae (2.27)–(2.32), y_5 and z_5 are respectively the horizontal and vertical centroidal axes of the cross-section of the beam, E_{B0} , η_{D0} , η_{L0} , and E_{H0} are respectively the values of E_B , η_D , η_L , and E_H in the upper left-hand vertex of the beam cross-section, and m_1 , n_1 , p_1 , and q_1 are respectively material properties that control the variation of E_B , η_D , η_L , and E_H along the width of the beam. The variation of E_B , η_D , η_L , and E_H along the thickness of the beam is controlled by the material properties: m_2 , n_2 , p_2 , and q_2 , respectively.

The variation of E_{B0} , E_{B1} , E_{B2} , η_{D0} , η_{D1} , η_{D2} , η_{L0} , η_{L1} , η_{L2} , E_{H0} , E_{H1} , and E_{H2} along the length of the beam is expressed as

$$(2.33) \quad E_{B0} = E_{B0R} + \frac{E_{B0T} - E_{B0R}}{l^{m_3}} x_5^{m_3},$$

$$(2.34) \quad E_{B1} = E_{B1R} + \frac{E_{B1T} - E_{B1R}}{l^{m_4}} x_5^{m_4},$$

$$(2.35) \quad E_{B2} = E_{B2R} + \frac{E_{B2T} - E_{B2R}}{l^{m_5}} x_5^{m_5},$$

$$(2.36) \quad \eta_{D0} = \eta_{D0R} + \frac{\eta_{D0T} - \eta_{D0R}}{l^{n_3}} x_5^{n_3},$$

$$(2.37) \quad \eta_{D1} = \eta_{D1R} + \frac{\eta_{D1T} - \eta_{D1R}}{l^{n_4}} x_5^{n_4},$$

$$(2.38) \quad \eta_{D2} = \eta_{D2R} + \frac{\eta_{D2T} - \eta_{D2R}}{l^{n_5}} x_5^{n_5},$$

$$(2.39) \quad \eta_{L0} = \eta_{L0R} + \frac{\eta_{L0T} - \eta_{L0R}}{l^{p_3}} x_5^{p_3},$$

$$(2.40) \quad \eta_{L1} = \eta_{L1R} + \frac{\eta_{L1T} - \eta_{L1R}}{l^{p_4}} x_5^{p_4},$$

$$(2.41) \quad \eta_{L2} = \eta_{L2R} + \frac{\eta_{L2T} - \eta_{L2R}}{l^{p_5}} x_5^{p_5},$$

$$(2.42) \quad E_{H0} = E_{H0R} + \frac{E_{H0T} - E_{H0R}}{l^{q_3}} x_5^{q_3},$$

$$(2.43) \quad E_{H1} = E_{H1R} + \frac{E_{H1T} - E_{H1R}}{l^{q_4}} x_5^{q_4},$$

$$(2.44) \quad E_{H2} = E_{H2R} + \frac{E_{H2T} - E_{H2R}}{l^{q_5}} x_5^{q_5},$$

where

$$(2.45) \quad 0 \leq x_5 \leq l.$$

In formulae (2.33)–(2.46), x_5 is the longitudinal centroidal axis of the beam, E_{B0R} , E_{B1R} , E_{B2R} , η_{D0R} , η_{D1R} , η_{D2R} , η_{L0R} , η_{L1R} , η_{L2R} , E_{H0R} , E_{H1R} , and E_{H2R} are respectively the values of E_{B0} , E_{B1} , E_{B2} , η_{D0} , η_{D1} , η_{D2} , η_{L0} , η_{L1} , η_{L2} , E_{H0} , E_{H1} , and E_{H2} at the free end of the beam, and E_{B0T} , E_{B1T} , E_{B2T} , η_{D0T} , η_{D1T} , η_{D2T} , η_{L0T} , η_{L1T} , η_{L2T} , E_{H0T} , E_{H1T} , and E_{H2T} are the values, respectively, of E_{B0} , E_{B1} , E_{B2} , η_{D0} , η_{D1} , η_{D2} , η_{L0} , η_{L1} , η_{L2} , E_{H0} , E_{H1} , and E_{H2} in the clamping. The variations of E_{B0} , E_{B1} , E_{B2} , η_{D0} , η_{D1} , η_{D2} , η_{L0} , η_{L1} , η_{L2} , E_{H0} , E_{H1} , and E_{H2} along the length of the beam are controlled by the material properties m_3 , m_4 , m_5 , n_3 , n_4 , n_5 , p_3 , p_4 , p_5 , q_3 , q_4 , and q_5 , respectively.

3. STRAIN ENERGY RELEASE RATE FOR THE LOWER CRACK

First, a time-dependent solution to the strain energy release rate that takes into account the viscoelastic behaviour of the inhomogeneous material is derived at an increase of the lower crack. For this purpose, the strain energy release rate G_{a_1} is written as

$$(3.1) \quad G_{a_1} = \frac{dU}{b da_1},$$

where U is the time-dependent strain energy in the beam structure.

Since the middle crack arm is free of stresses, the strain energy is found as

$$(3.2) \quad U = U_1 + U_2 + U_3 + U_4,$$

where U_1 , U_2 , U_3 , and U_4 are the strain energies cumulated in the lower crack arm, in the beam portion S_2S_3 of the upper crack arm, in the portion S_1S_2 of the upper crack arm and in the uncracked beam portion $a_1 \leq x_5 \leq l$, respectively.

The strain energy in the lower crack arm is obtained as

$$(3.3) \quad U_1 = \int_0^{a_1} \int_{-\frac{b}{2}}^{\frac{b}{2}} \int_{-\frac{h_1}{2}}^{\frac{h_1}{2}} u_{01} dx_5 dy_1 dz_1,$$

where u_{01} is the time-dependent strain energy density in the lower crack arm, and y_1 and z_1 are the centroidal axes of the cross-section of the crack arm (Fig. 3).

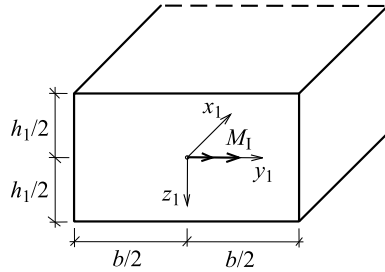


FIG. 3. Cross-section of the lower crack arm.

The time-dependent strain energy is expressed as

$$(3.4) \quad u_{01} = \frac{1}{2} \sigma \varepsilon.$$

The distribution of strains is treated by applying the Bernoulli's hypothesis for plane sections since beams of high length to thickness ratio are under consideration in the present paper. Therefore, the distribution of ε in the cross-section of the lower crack arm is written as

$$(3.5) \quad \varepsilon = \varepsilon_{C_1} + \kappa_{y_1} y_1 + \kappa_{z_1} z_1,$$

where ε_{C_1} is the strain in the centre of the cross-section of the lower crack arm, and κ_{y_1} and κ_{z_1} are the curvatures in $x_1 y_1$ and $x_1 z_1$ coordinate planes, respectively. The quantities ε_{C_1} , κ_{y_1} , and κ_{z_1} are determined by using the following equations for equilibrium of the elementary forces in the cross-section of the lower crack arm:

$$(3.6) \quad N_1 = \iint_{(A_1)} \sigma \, dA,$$

$$(3.7) \quad M_{y_1} = \iint_{(A_1)} \sigma z_1 \, dA,$$

$$(3.8) \quad M_{z_1} = \iint_{(A_1)} \sigma y_1 \, dA,$$

where A_1 is the area of the cross-section, N_1 is the axial force, and M_{y_1} and M_{z_1} are the bending moments with respect to y_1 and z_1 axes. It is obvious that

$$(3.9) \quad N_1 = 0,$$

$$(3.10) \quad M_{y_1} = M_I,$$

$$(3.11) \quad M_{z_1} = 0.$$

At $0 \leq t \leq t_1$, the stress-strain-time relationship (2.18) is used. By combining (2.18) and (3.5), one obtains

$$(3.12) \quad \sigma = (\varepsilon_{C_1} + \kappa_{y_1}y_1 + \kappa_{z_1}z_1) \cdot \left[\frac{1}{\theta^2 t} \left(\frac{1}{\eta_L} - \frac{\beta}{\theta} \right) (e^{-\theta t} - 1) + \frac{\beta}{2\theta} t + \frac{1}{\theta} \left(\frac{1}{\eta_L} - \frac{\beta}{\theta} \right) + \frac{1}{E_H} \right]^{-1}.$$

After substituting of (3.12) in (3.6), (3.7), and (3.8), the three equations for equilibrium are solved with respect to ε_{C_1} , κ_{y_1} and κ_{z_1} at various values of time by using the MatLab computer program.

The time-dependent strain energy density in the lower crack arm is obtained by combining (3.4), (3.5), and (3.12). The result is

$$(3.13) \quad u_{01} = \frac{1}{2}(\varepsilon_{C_1} + \kappa_{y_1}y_1 + \kappa_{z_1}z_1)^2 \cdot \left[\frac{1}{\theta^2 t} \left(\frac{1}{\eta_L} - \frac{\beta}{\theta} \right) (e^{-\theta t} - 1) + \frac{\beta}{2\theta} t + \frac{1}{\theta} \left(\frac{1}{\eta_L} - \frac{\beta}{\theta} \right) + \frac{1}{E_H} \right]^{-1}.$$

The strain energy in portion S_2S_3 of the upper crack arm is written as

$$(3.14) \quad U_2 = \int_{a_2 - \frac{b}{2} - \frac{h_4}{2}}^{a_1} \int_{-\frac{b}{2}}^{\frac{b}{2}} \int_{-\frac{h_4}{2}}^{\frac{h_4}{2}} u_{02} dx_5 dy_2 dz_2,$$

where u_{02} is the time-dependent strain energy density in this crack arm, and y_2 and z_2 are the centroidal axes of the cross-section of the crack arm.

Formula (3.13) is applied also to calculate u_{02} . For this purpose, ε_{C_1} , κ_{y_1} , κ_{z_1} , y_1 , and z_1 are replaced with ε_{C_2} , κ_{y_2} , κ_{z_2} , y_2 , and z_2 , respectively, where ε_{C_2} is the strain in the centre of the cross-section, and κ_{y_2} and κ_{z_2} are the curvatures of the crack arm. Equations (3.6), (3.7), and (3.8) are used to determine ε_{C_2} , κ_{y_2} , and κ_{z_2} . For this purpose, A_1 , σ , y_1 , z_1 , and M_{y_1} are replaced with A_2 , $\sigma_{S_2S_3}$, y_2 , z_2 , and M_{II} , respectively, where A_2 is the area of the cross-section of this crack arm, and $\sigma_{S_2S_3}$ is the stress. Formula (3.12) is applied to determine $\sigma_{S_2S_3}$ by replacing of ε_{C_1} , κ_{y_1} , κ_{z_1} , y_1 , and z_1 with ε_{C_2} , κ_{y_2} , κ_{z_2} , y_2 , and z_2 , respectively.

The strain energy in the portion S_1S_2 of the upper crack arm is found as

$$(3.15) \quad U_3 = \int_0^{a_2} \int_{-\frac{b}{2}}^{\frac{b}{2}} \int_{-\frac{h_3}{2}}^{\frac{h_3}{2}} u_{03} dx_5 dy_3 dz_3,$$

where the time-dependent strain energy density u_{03} is derived by replacing ε_{C_1} , κ_{y_1} , κ_{z_1} , y_1 , and z_1 with ε_{C_3} , κ_{y_3} , κ_{z_3} , y_3 , and z_3 , respectively, in (3.13). After performing the necessary replacements, equations (3.6), (3.7), and (3.8) are used to determine ε_{C_3} , κ_{y_3} , and κ_{z_3} .

The strain energy in the uncracked portion of the beam is obtained as

$$(3.16) \quad U_4 = \int_{a_1}^l \int_{-\frac{b}{2}}^{\frac{b}{2}} \int_{-\frac{h}{2}}^{\frac{h}{2}} u_{04} dx_5 dy_4 dz_4,$$

where u_{04} is the time-dependent strain energy density, and y_4 and z_4 are the centroidal axes of the cross-section of the un-cracked beam portion. The time-dependent strain energy density is found by replacing ε_{C_1} , κ_{y_1} , κ_{z_1} , y_1 , and z_1 with ε_{C_4} , κ_{y_4} , κ_{z_4} , y_4 , and z_4 , respectively, in (3.13). Equations (3.6), (3.7), and (3.8) are applied to obtain ε_{C_4} , κ_{y_4} , and κ_{z_4} after the corresponding replacements.

The following time-dependent solution to the strain energy release rate is derived by combining (3.1), (3.2), (3.3), (3.14), (3.15), and (3.16):

$$(3.17) \quad G_{a_1} = \frac{1}{b} \left(\int_{-\frac{b}{2}}^{\frac{b}{2}} \int_{-\frac{h_1}{2}}^{\frac{h_1}{2}} u_{01} dy_1 dz_1 + \int_{-\frac{b}{2}}^{\frac{b}{2}} \int_{-\frac{h_4}{2}}^{\frac{h_4}{2}} u_{02} dy_2 dz_2 - \int_{-\frac{b}{2}}^{\frac{b}{2}} \int_{-\frac{h}{2}}^{\frac{h}{2}} u_{04} dy_4 dz_4 \right),$$

where the strain energy densities are obtained at $x_5 = a_1$. Formula (3.17) is used to calculate the strain energy release rate at various values of time. The integration is carried out by the MatLab computer program. It should be noted that (3.17) is valid at $0 \leq t \leq t_1$.

The time-dependent strain energy release rate at $0 \leq t \leq t_1$ is also obtained by considering the balance of energy

$$(3.18) \quad M_I \delta \varphi_I + M_{II} \delta \varphi_{II} = \frac{\partial U}{\partial a_1} \delta a_1 + G_{a_1} b \delta a_1,$$

where $\delta \varphi_I$ and $\delta \varphi_{II}$ are the increases of angles of rotation of free ends of the lower and upper crack arms, respectively, and δa_1 is a small increase of the lower crack. From (3.18), one derives

$$(3.19) \quad G_{a_1} = \frac{M_I}{b} \frac{\partial \varphi_I}{\partial a_1} + \frac{M_{II}}{b} \frac{\partial \varphi_{II}}{\partial a_1} - \frac{1}{b} \frac{\partial U}{\partial a_1}.$$

The angles of rotation φ_I and φ_{II} are found by applying the theorem of Castigliano

$$(3.20) \quad \varphi_I = \frac{\partial U}{\partial M_I},$$

$$(3.21) \quad \varphi_{II} = \frac{\partial U}{\partial M_{II}}.$$

By substituting (3.2), (3.3), (3.14)–(3.16), (3.20), and (3.21) in (3.19), one obtains

$$(3.22) \quad G_{a_1} = \frac{M_I}{b} \frac{\partial}{\partial M_I} \left(\int_{-\frac{b}{2}}^{\frac{b}{2}} \int_{-\frac{h_1}{2}}^{\frac{h_1}{2}} u_{01} dy_1 dz_1 - \int_{-\frac{b}{2}}^{\frac{b}{2}} \int_{-\frac{h}{2}}^{\frac{h}{2}} u_{04} dy_4 dz_4 \right) \\ + \frac{M_{II}}{b} \frac{\partial}{\partial M_{II}} \left(\int_{-\frac{b}{2}}^{\frac{b}{2}} \int_{-\frac{h_4}{2}}^{\frac{h_4}{2}} u_{02} dy_2 dz_2 - \int_{-\frac{b}{2}}^{\frac{b}{2}} \int_{-\frac{h}{2}}^{\frac{h}{2}} u_{04} dy_4 dz_4 \right) \\ - \frac{1}{b} \left(\int_{-\frac{b}{2}}^{\frac{b}{2}} \int_{-\frac{h_1}{2}}^{\frac{h_1}{2}} u_{01} dy_1 dz_1 + \int_{-\frac{b}{2}}^{\frac{b}{2}} \int_{-\frac{h_4}{2}}^{\frac{h_4}{2}} u_{02} dy_2 dz_2 - \int_{-\frac{b}{2}}^{\frac{b}{2}} \int_{-\frac{h}{2}}^{\frac{h}{2}} u_{04} dy_4 dz_4 \right),$$

where the strain energy densities are found at $x_5 = a_1$. The integration in (3.22) is carried out by the MatLab computer program. The derivatives $\frac{\partial}{\partial M_I}(\dots)$ and $\frac{\partial}{\partial M_{II}}(\dots)$ in (3.22) are obtained by the MatLab computer program. Formula (3.22) is used to calculate the strain energy release rate at various values of time. It should be mentioned that the strain energy release rates obtained by (3.22) are exact matches of those found by (3.17). This fact proves the correctness of the solutions derived.

Formula (3.17) is also applied to calculate the strain energy release rate at $t \geq t_1$. In this case, the stress-strain-time relationship (2.26) is used. First, the time-dependent strain energy density in the lower crack arm is found. By using (2.26) and (3.5), one derives

$$(3.23) \quad \sigma = (\varepsilon_{C_1} + \kappa_{y_1} y_1 + \kappa_{z_1} z_1) \\ \cdot \left(\xi - \frac{\delta - \theta \zeta}{\theta^2} - \frac{\delta}{\theta} t_1 + \frac{\delta - \theta \zeta}{\theta^2 e^{-\theta t_1}} e^{-\theta t} + \frac{\delta}{\theta} t + \frac{1}{E_H} \right)^{-1}.$$

By combining (3.4), (3.5), and (3.23), one obtains the following expression for the time-dependent strain energy density in the lower crack arm:

$$(3.24) \quad u_{01} = \frac{1}{2}(\varepsilon_{C_1} + \kappa_{y_1}y_1 + \kappa_{z_1}z_1)^2 \cdot \left(\xi - \frac{\delta - \theta\zeta}{\theta^2} - \frac{\delta}{\theta}t_1 + \frac{\delta - \theta\zeta}{\theta^2 e^{-\theta t_1}} e^{-\theta t} + \frac{\delta}{\theta}t + \frac{1}{E_H} \right)^{-1}.$$

Equations for equilibrium (3.6), (3.7), and (3.8) are used to determine ε_{C_1} , κ_{y_1} , and κ_{z_1} . For this purpose, after substituting (3.23) in (3.6)–(3.8), the equations for equilibrium are solved with respect to ε_{C_1} , κ_{y_1} , and κ_{z_1} at various values of time by the MatLab computer program.

Formula (3.24) is also used to calculate the time-dependent strain energy density in the portion S_2S_3 of the upper crack arm by replacing ε_{C_1} , κ_{y_1} , κ_{z_1} , y_1 and z_1 with ε_{C_2} , κ_{y_2} , κ_{z_2} , y_2 and z_2 , respectively. The quantities ε_{C_2} , κ_{y_2} , and κ_{z_2} are determined from Eqs. (3.6)–(3.8) after carrying out the necessary replacements.

The time-dependent strain energy density in the portion S_1S_2 of the upper crack arm is found by replacing ε_{C_1} , κ_{y_1} , κ_{z_1} , y_1 and z_1 with ε_{C_3} , κ_{y_3} , κ_{z_3} , y_3 and z_3 , respectively, in (3.24). Equations (3.6)–(3.8) are used to determine ε_{C_3} , κ_{y_3} , κ_{z_3} after corresponding replacements.

The quantities ε_{C_1} , κ_{y_1} , κ_{z_1} , y_1 and z_1 , are replaced with ε_{C_4} , κ_{y_4} , κ_{z_4} , y_4 and z_4 , respectively, in (3.24) in order to derive the time-dependent strain energy density in the uncracked beam portion. Analogical replacements are carried out in equilibrium Eqs. (3.6)–(3.8) to determine ε_{C_4} , κ_{y_4} , and κ_{z_4} .

After substituting of the time-dependent strain energy densities in (3.17), the integration is performed by the MatLab computer program. Formula (3.17) is applied to calculate the strain energy release rate at various values of time.

The strain energy release rate at $t \geq t_1$ is also obtained by considering the energy balance. For this purpose, formula (3.22) is applied. After substituting of the time-dependent strain energy densities found by using (3.24) in (3.22), the integration is performed by the MatLab computer program at various values of time. The fact that the strain energy release rates found by (3.22) are exact matches of those obtained by (3.17) confirms the correctness of the solutions derived.

4. STRAIN ENERGY RELEASE RATE FOR THE UPPER CRACK

The strain energy release rate is also found at an increase of the upper crack. For this purpose, a_1 is replaced with a_2 in formula (3.1). By substituting (3.3), (3.14), (3.15) and (3.16) in (3.2) and then in (3.1), one obtains

$$(4.1) \quad G_{a_2} = \frac{1}{b} \left(\int_{-\frac{b}{2}}^{\frac{b}{2}} \int_{-\frac{h_3}{2}}^{\frac{h_3}{2}} u_{03} \, dy_3 \, dz_3 - \int_{-\frac{b}{2}}^{\frac{b}{2}} \int_{-\frac{h_4}{2}}^{\frac{h_4}{2}} u_{02} \, dy_2 \, dz_2 \right),$$

where the time-dependent strain energy densities are found by (3.13). The integration in (4.1) is carried out by the MatLab computer program. Formula (4.1) is used to calculate the strain energy release rate at various values of time. It should be noted that (4.1) is applicable at $0 \leq t \leq t_1$.

A time-dependent solution to the strain energy release rate for $0 \leq t \leq t_1$ is also obtained by considering the balance of energy at an increase of the upper crack arm. For this purpose, a_1 is replaced with a_2 in (3.19). By substituting (3.3), (3.14), (3.15) and (3.16) in (3.20) and (3.21) and then in (3.19), one derives

$$(4.2) \quad G_{a_2} = \frac{M_{II}}{b} \frac{\partial}{\partial M_{II}} \left(\int_{-\frac{b}{2}}^{\frac{b}{2}} \int_{-\frac{h_3}{2}}^{\frac{h_3}{2}} u_{03} \, dy_3 \, dz_3 - \int_{-\frac{b}{2}}^{\frac{b}{2}} \int_{-\frac{h_4}{2}}^{\frac{h_4}{2}} u_{02} \, dx_5 \, dy_2 \, dz_2 \right) \\ \cdot - \frac{1}{b} \left(\int_{-\frac{b}{2}}^{\frac{b}{2}} \int_{-\frac{h_3}{2}}^{\frac{h_3}{2}} u_{03} \, dy_3 \, dz_3 - \int_{-\frac{b}{2}}^{\frac{b}{2}} \int_{-\frac{h_4}{2}}^{\frac{h_4}{2}} u_{02} \, dy_2 \, dz_2 \right).$$

The integration in (4.2) is performed by using the MatLab computer program. It should be noted that the strain energy release rate obtained by (4.2) are identical with those found by (4.1), which proves the correctness of the analysis.

Formula (4.1) is also applied to calculate the time-dependent strain energy release rate for $t \geq t_1$ at an increase of the upper crack. For this purpose, the time-dependent strain energy densities obtained by using (3.24) are substituted in (4.1). The integration is carried out by the MatLab computer program.

Calculations of the time-dependent strain energy release rate for $t \geq t_1$ at an increase of the upper crack are also carried out by (4.2). After substituting the time-dependent strain energy densities found by (3.24) in (4.2), the integration is performed by the MatLab computer program. The results obtained by (4.1) and (4.2) are identical. This fact proves the correctness of the solutions derived.

5. PARAMETRIC INVESTIGATION

A parametric investigation is performed by applying the time-dependent solutions to the strain energy release rate derived in Secs 3 and 4 of the present paper. The strain energy release rate is expressed in non-dimensional form by

using the formula $G_N = G/(E_{B0R}b)$. The basic purpose of the parametric investigation is to evaluate the effects of the viscoelastic behaviour of the material on the strain energy release rate in the inhomogeneous beam configuration with two lengthwise cracks shown in Fig. 1. It is assumed that $b = 0.015$ m, $h = 0.020$ m, $l = 0.300$ m, $m_i = 0.7$, $n_i = 0.7$, $p_i = 0.7$, $q_i = 0.7$, where $i = 1, 2, \dots, 5$, $v_I = 1.25 \cdot 10^{-5}$ N · m/s, and $v_{II} = 0.75 \cdot 10^{-5}$ N · m/s.

First, the variation of the strain energy release rate with time is analysed at an increase of the lower crack. Calculations are carried out by applying the solution (3.17). The strain energy release rate in non-dimensional form is plotted against the non-dimensional time in Fig. 4. The time is presented in non-dimensional form by using the formula $t_N = tE_{B0R}/\eta_{D0R}$. It can be observed in Fig. 4 that the strain energy release rate increases with time (this is due to the viscoelastic behaviour of the material). One can also observe that the curve is steeper at $0 \leq t \leq t_1$ (Fig. 4). This finding is attributed to the increase of the bending moments at $0 \leq t \leq t_1$ while at $t \geq t_1$ the bending moments remain constants (the increase of the strain energy release rate at $t \geq t_1$ is due to creep under constant loading).

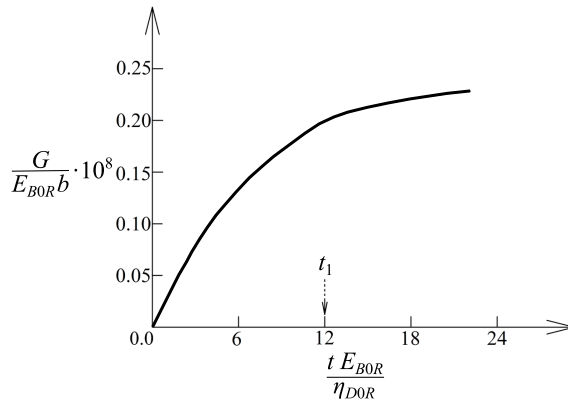


FIG. 4. The strain energy release rate in non-dimensional form plotted against the non-dimensional time at an increase of the lower crack.

The influences of the continuous variation of E_B along the beam width and the location of the lower crack along the beam thickness on the strain energy release rate are investigated at the increase of the lower crack. For this purpose, calculations are performed at various E_{B1}/E_{B0} and h_1/h ratios. One can get an idea about these influences from Fig. 5, where the strain energy release rate in non-dimensional form is plotted against E_{B1}/E_{B0} ratio at three h_1/h ratios. The curves in Fig. 5 indicate that the strain energy release rate decreases with increasing of E_{B1}/E_{B0} ratio. The increase of h_1/h ratio also leads to a decrease of the strain energy release rate (Fig. 5).

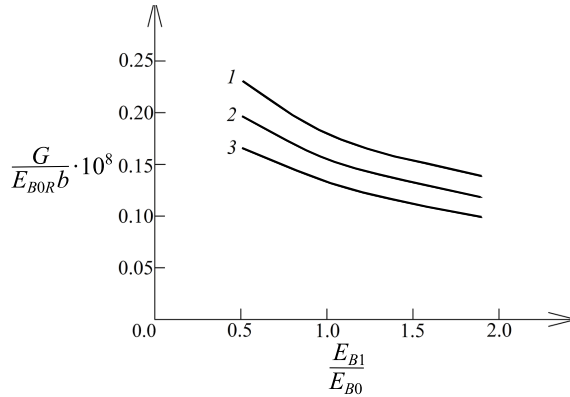


FIG. 5. The strain energy release rate in non-dimensional form plotted against E_{B1}/E_{B0} ratio at an increase of the lower crack (curve 1 – at $h_1/h = 0.1$, curve 2 – at $h_1/h = 0.2$, and curve 3 – at $h_1/h = 0.3$).

The effects of the crack length and the continuous variation of η_D along the beam thickness are investigated too. Calculations are carried out at various a_1/l and η_{D2}/η_{D0} ratios. The results of these calculations are illustrated in Fig. 6, where the strain energy release rate in non-dimensional form is plotted against η_{D2}/η_{D0} ratio at three a_1/l ratios. One can observe in Fig. 6 that the strain energy release rate decreases with increasing of η_{D2}/η_{D0} ratio. It can also be observed in Fig. 6 that the increase of a_1/l ratio leads to an increase of the strain energy release rate.

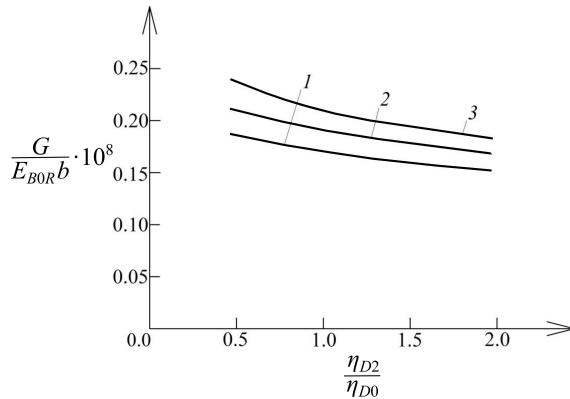


FIG. 6. The strain energy release rate in non-dimensional form plotted against η_{D2}/η_{D0} ratio at increase of the lower crack (curve 1 – at $a_1/l = 0.30$, curve 2 – at $a_1/l = 0.50$, and curve 3 – at $a_1/l = 0.70$).

Calculations of the strain energy release rate are also performed at various η_{L0T}/η_{L0R} and E_{H0T}/E_{H0R} ratios in order to analyse the influence of the conti-

nuous variation of η_{L0} and E_{H0} along the beam length. The strain energy release rate in non-dimensional form is plotted against η_{L0T}/η_{L0R} ratio in Fig. 7 at three E_{H0T}/E_{H0R} ratios. The curves in Fig. 7 reveal that the strain energy release rate decreases with increasing of η_{L0T}/η_{L0R} ratio. One can observe in Fig. 7 that the increase of E_{H0T}/E_{H0R} ratio also leads to a decrease in the strain energy release rate.

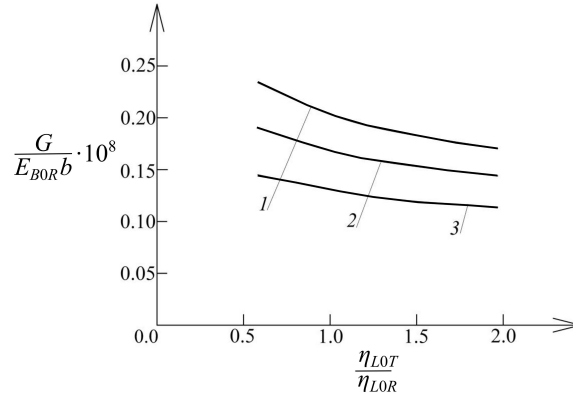


FIG. 7. The strain energy release rate in non-dimensional form plotted against η_{L0T}/η_{L0R} ratio at an increase of the lower crack (curve 1 – at $E_{H0T}/E_{H0R} = 0.5$, curve 2 – at $E_{H0T}/E_{H0R} = 1.0$, and curve 3 – at $E_{H0T}/E_{H0R} = 2.0$).

The variation of the strain energy release rate with time at an increase of the upper crack arm is also studied. For this purpose, the strain energy release rate in non-dimensional form is plotted against the non-dimensional time in Fig. 8. The curve in Fig. 8 shows that the strain energy release rate decreases with time. It can be observed in Fig. 8 that at $0 \leq t \leq t_1$ the curve is steeper than at $t \geq t_1$.

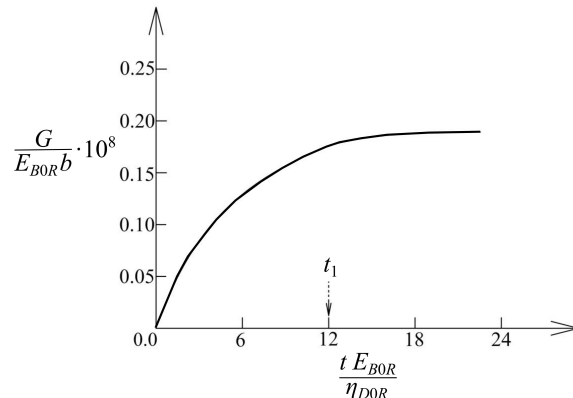


FIG. 8. The strain energy release rate in non-dimensional form plotted against the non-dimensional time at an increase of the upper crack.

The influences of the continuous variations of η_D and η_L along the beam width on the strain energy release rate at increase of the upper crack are analysed by performing calculations at various η_{D1}/η_{D0} and η_{L1}/η_{L0} ratios. The results obtained are shown in Fig. 9, where the strain energy release rate in non-dimensional form is plotted against η_{D1}/η_{D0} ratio at three η_{L1}/η_{L0} ratios. One can observe in Fig. 9 that the strain energy release rate decreases with increasing of η_{D1}/η_{D0} and η_{L1}/η_{L0} ratios.

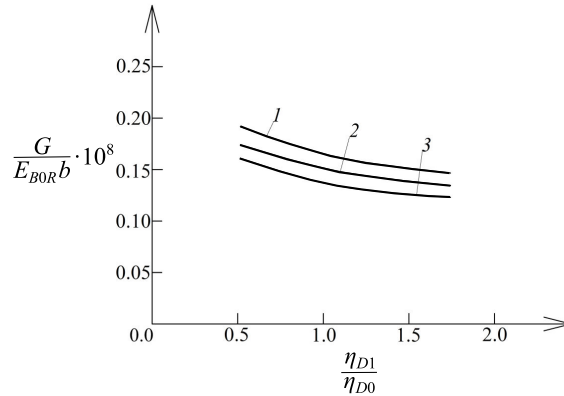


FIG. 9. The strain energy release rate in non-dimensional form plotted against η_{D1}/η_{D0} ratio at an increase of the upper crack (curve 1 - at $\eta_{L1}/\eta_{L0} = 0.5$, curve 2 - at $\eta_{L1}/\eta_{L0} = 1.0$, and curve 3 - at $\eta_{L1}/\eta_{L0} = 2.0$).

The effect of continuous variation of E_H along the beam thickness on the strain energy release rate is investigated. For this purpose, calculations of the strain energy release rate are carried out at various E_{H2}/E_{H0} ratios by applying solutions (3.17) and (4.1). The strain energy release rate in non-dimensional form is plotted against E_{H2}/E_{H0} ratio in Fig. 10. The curves in Fig. 10 show

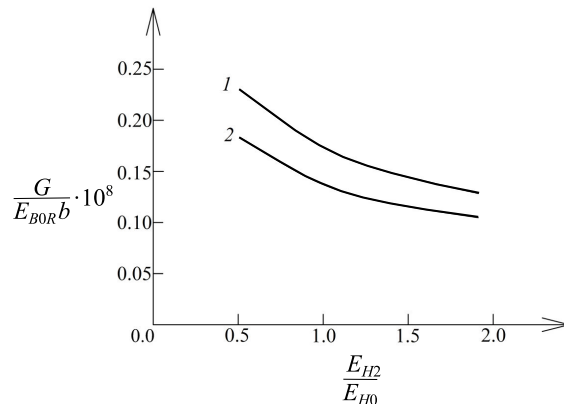


FIG. 10. The strain energy release rate in non-dimensional form plotted against E_{H2}/E_{H0} ratio (curve 1 - at an increase of the lower crack, curve 2 - at an increase of the upper crack).

that the strain energy release rate decreases with increasing of E_{H2}/E_{H0} ratio. One can also observe in Fig. 10 that the strain energy release rate derived at an increase of the lower crack is higher than that at an increase of the upper crack.

6. CONCLUSION

A viscoelastic continuously inhomogeneous beam configuration with two lengthwise cracks was analysed. The viscoelastic behaviour was examined by using a rheological model with two springs and two dashpots. A stress-strain-time relationship was derived assuming that the rheological model is loaded by stress that increases linearly with time up to a certain magnitude and then the stress is kept constant. Since the beam exhibits continuous material inhomogeneity in the width, thickness and length directions, the moduli of elasticity of the springs and the coefficients of the viscosity of the dashpots vary continuously in the volume of the beam. A solution to the strain energy release rate was obtained by analysing the time-dependent strain energy cumulated in the beam. The strain energy release rate was also found by considering the balance of energy. The two solutions produce identical results. This fact proves the correctness of the solutions derived. The variation of the strain energy release rate with time was analysed. It was found that the strain energy release rate increases with time. The analysis revealed that the strain energy release rate – time curve at $0 \leq t \leq t_1$ is steeper than at $t \geq t_1$. This behaviour is due to the increase of the bending moments in the beam at $0 \leq t \leq t_1$ while at $t \geq t_1$ the bending moments do not change. Actually, the increase of the strain energy release rate at $t \geq t_1$ is caused by creep under constant external loading applied on the beam. The effects of the length and the location of the lower crack along the beam thickness were evaluated. It was found that the strain energy release rate decreases with increasing of h_1/h ratio. The increase of a_1/l ratio leads to an increase in the strain energy release rate. The influence of the material inhomogeneity on the strain energy release rate was analysed. The analysis indicates that the strain energy release rate decreases with increasing of E_{B1}/E_{B0} , η_{D2}/η_{D0} , η_{L0T}/η_{L0R} , E_{H0T}/E_{H0R} , η_{D1}/η_{D0} , η_{L1}/η_{L0} , and E_{H2}/E_{H0} ratios. The investigation showed that the strain energy release rate for the lower crack was higher than that for the upper crack.

REFERENCES

1. KOIZUMI M., The concept of FGM, *Ceramic Transactions, Functionally Gradient Materials*, **34**(2): 3–10, 1993.
2. NEUBRAND A., RÖDEL J., Gradient materials: An overview of a novel concept, *Zeitschrift für Metallkunde*, **88**(5): 358–371, 1997.

3. GASIK M.M., Functionally graded materials: bulk processing techniques, *International Journal of Materials and Product Technology*, **39**(1–2): 20–29, 2010, doi: 10.1504/IJMPT.2010.034257.
4. RABENDA M., Analysis of non-stationary heat transfer in a hollow cylinder with functionally graded material properties performed by different research methods, *Engineering Transactions*, **63**(3): 329–339, 2015.
5. RAMESH MAGANTI N.V., MOHAN RAO NALLURI, Flapwise bending vibration analysis of functionally graded rotating double-tapered beams, *International Journal of Mechanical and Materials Engineering*, **10**(1): 21, 2015, doi: 10.1186/s40712-015-0040-0.
6. KEDDOURI A., HADJI L., TOUNSI A., Static analysis of functionally graded sandwich plates with porosities, *Advances in Materials Research*, **8**(3): 155–177, 2019, doi: 10.12989/amr.2019.8.3.155.
7. BOHIDAR S.K., SHARMA R., MISHRA P.R., Functionally graded materials: A critical review, *International Journal of Research*, **1**(4): 289–301, 2014.
8. MAHAMOOD R.M., AKINLABI E.T., *Functionally Graded Materials*, Springer, 2017.
9. RIZOV V.I., Analytical study of elastic-plastic longitudinal fracture in a functionally graded beam, *Strength, Fracture and Complexity*, **10**(1): 11–22, 2017, doi: 10.3233/SFC-170197.
10. RIZOV V.I., Analysis of delamination in two-dimensional functionally graded multilayered beam with non-linear behaviour of material, *Engineering Transactions*, **66**(1): 61–78, 2018.

Received July 14, 2020; accepted version September 6, 2020.

Published on Creative Common licence CC BY-SA 4.0

